A Microwave Imaging System for Inline Food Inspection

(Article begins on next page)

A Microwave Imaging System for Inline Food Inspection

Calin Ion Maraloiu
Dept. Electronics and Telecommunications
Politecnico di Torino
Torino, Italy
calin.maraloiu@polito.it

Juan Felipe González-Pardo
Dept. Electronics and Telecommunications
Politecnico di Torino
Torino, Italy
juan.gonzalez@polito.it

Jorge Alberto Tobon Vasquez
Wavision srl
Torino, Italy
jorge.tobon@wavision.it

Marco Ricci
Wavision srl
Torino, Italy
marco.ricci@wavision.it

Francesca Vipiana
Dept. Electronics and Telecommunications
Politecnico di Torino
Torino, Italy
francesca.vipiana@polito.it

***Abstract*—Microwave imaging (MWI) is a promising technology that can be exploited for the industrial development of real-time, noninvasive and nondestructive inline inspection systems, in the context of foreign body detection. Here, the aim is to assess the use of MWI to detect the presence of physical contaminants within packaged food products, through the retrieval of 3D images displaying the dielectric contrast of the analyzed item. For this purpose, we propose a microwave imaging system made of an antenna array to scan the tested product and detect the interaction of the contaminant with the incident electromagnetic signal. The designed antennas are wide-band horn antennas placed along the production line and around the item under test. Then, a numerical validation of the implemented inversion operators is detailed for a dynamic scenario. The obtained results offer a potentially effective outcome for a practical implementation and testing of the proposed system on production lines.**

***Index Terms*—Food safety, microwave antenna arrays, microwave imaging, microwave propagation.**

I. Introduction

In the food processing industry, physical contamination is a threat for quality and consumers health. Additionally, it can lead to a significant reduction in sales with negative effects on the public's perception of the product. For this reason, it is essential to integrate fast and accurate technologies, capable of performing inspections, without interfering or reducing production capacity. Inspection systems, such as x-ray and metal detectors, have been well incorporated for these cases. However, typical intrusion materials, such as glass, wood, or plastic, being non-metallic or low density, are not properly detected with these commercially available machines.

In recent years, microwave imaging technology has demonstrated its ability to overcome these limitations [1]–[4]. Contaminants alter the incident field, resulting in small variations in the scattering parameters. These are sensed by an array of transmitting and receiving antennas and can be translated into 3D dielectric contrast maps [5], [6]. The advantages of MWI inspection systems rely on their adaptability, portability, and low maintenance requirements. The performance of MWI devices, integrated to a production line, depends on several aspects, including the design of the radiating elements, the configuration of the antenna array and the inversion strategies used for the image reconstruction. Firstly, the antenna should have a wide bandwidth over an appropriate frequency range, while maintaining a compact size. Secondly, the array setup has to ensure proper coverage within the imaging domain, allowing the inversion algorithm to reconstruct the dielectric contrast and the contaminant location.

In this work, we present the numerical validation of a MWI system, which integrates six tailored extended gap ridged slotted horn (EGRSH) antennas [7], [8], arranged in an arch configuration for the inspection of oil-based products. For this purpose, the truncated singular value decomposition (TSVD) algorithm is used with multi-frequency and multi-position approaches to locate contaminants correctly.

II. Design of the MWI system

The geometry of the antenna array is reported in Fig. 1 (a) and presents a complete picture of the MWI system design. It comprises a set of six horn antennas, which are placed in a configuration capable of scanning industrial products moving along the x-axis. This setup optimizes their disposition around the upper part of the perimeter of the tested item cross section. Due to industrial constraints related to the object motion, it is not possible to place antennas facing the jar along the x-direction. As a consequence, the antennas are not able to properly scan the whole target length in the direction of movement. This could lead to badly covered front and back portions of the product. Moreover, due to the limited resolution along the xz-plane, caused by the absence of antennas, the array might not be able to properly focus the shape of the intrusion. This can generate elongated shape reconstructions of the detected high contrast region along the x-direction. To solve these issues, motion can be exploited to

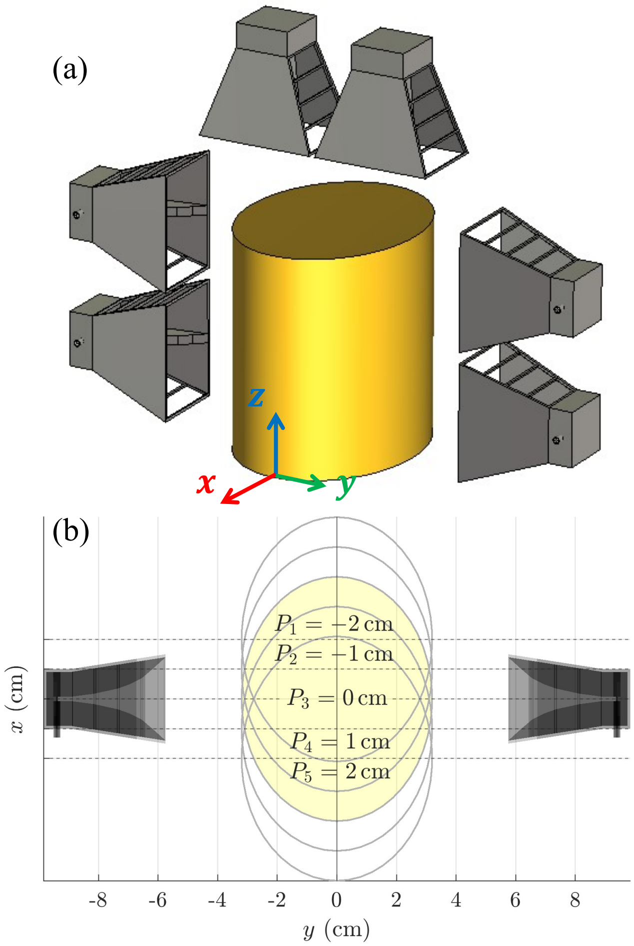

Figure 1. Proposed MWI setup (a) including the six EGRHS antennas, disposed in an arch configuration arranged around the inspected product and overview (b) of the simulated dynamic scenario along the motion axis.

build a multi-position scenario, which allows compensating for the coverage lack in the problematic regions. As shown in Fig. 1 (b), we study five equi-spaced scenarios, accounting for a total dynamic displacement interval of $x = (0 \pm 2)$ cm along the motion axis. For imaging purposes, the behavior of the antenna array has been analyzed in the frequency range $6 - 11$ GHz, with 1 GHz of step, to take advantage of its ultra-wideband (UWB) features. The radiating element is a compact $43 \times 40 \times 41$ mm EGRSH antenna, consisting of a waveguide launcher with ridge transitions inside a slotted horn cavity, and fed by a coaxial line. The designed antenna has been numerically validated in the $6-11$ GHz range, providing an appropriate penetration depth and coverage for oil-based products, packaged in glass containers [7]. Horn antennas are well known for their focused radiation patterns, which are preferred for this application compared to omnidirectional antennas.

The trial product, discussed in this paper, is an elliptical base cylinder, that mimics conventional oil-based spread jars, commonly available on the market. It has a 4.2 cm semi-major axis, a 3.1 cm semi-minor axis and a length of 8.0 cm. The material in the jar is oil, whose relative permittivity and conductivity are reported in Table I for the considered frequency range.

III. Validation of the Imaging Inversion Operators

The goal of microwave imaging is to retrieve information about the dielectric contrast $\Delta\chi$, expressed as the difference of the positional dielectric permittivity $\epsilon(\mathbf{r})$, computed in each point $\mathbf{r}$ of the investigation domain, and the background medium permittivity ϵ_b, all scaled over the latter:

$$\Delta\chi(\mathbf{r}) = \frac{\epsilon(\mathbf{r}) - \epsilon_b}{\epsilon_b}. \tag{1}$$

The differential scattering matrix ΔS at the antennas' ports (of size $6 \times 6 \times 5$, corresponding to the mutual interactions of the 6 antennas acquired over the 5 considered positions) is obtained as the difference between the uncontaminated (jar filled just with the background material) and the contaminated scenarios, since the goal is to search for the perturbation on the incident wave caused by the contaminant. The dielectric contrast $\Delta\chi(\mathbf{r})$ has to be retrieved through an inversion procedure [3]. The computation of the mathematical operator $\mathcal{L}$, which is the link between $\Delta\chi(\mathbf{r})$ and ΔS, cannot be done in closed form, hence the discretized problem is derived

$$[\Delta S] = [L][\Delta\chi], \tag{2}$$

where the original differential matrix ΔS is reshaped into a $[\Delta S]$ column vector. Conversely, $[L]$ is the discretized imaging operator and $[\Delta\chi]$ is the discretized dielectric contrast computed over the mesh elements that sample the domain of interest. The $[L]$ operator is computed offline from the simulation of an uncontaminated scenario, considering the material properties shown in Table I. For the inversion procedure, the TSVD method is applied to (2) to retrieve the dielectric contrast $[\Delta\chi]$:

$$[\Delta\chi] = \sum_{n=1}^{T} \frac{1}{\sigma_n} \langle [\Delta S], [u_n] \rangle [v_n], \tag{3}$$

where σ_n is the nth singular value, $[u_n]$ and $[v_n]$ are respectively the nth left singular vector and right singular vector, obtained from the SVD factorization of the $[L]$ operator. T is the truncation index, and corresponds to the number of singular values retained to construct a rank-n approximation.

Table I
Measured values of oil relative permittivity and conductivity

f (GHz)	6.0	7.0	8.0	9.0	10.0	11.0
ϵ_r	2.65	2.61	2.60	2.59	2.56	2.55
σ (S/m)	0.04	0.02	0.01	0.04	0.04	0.04

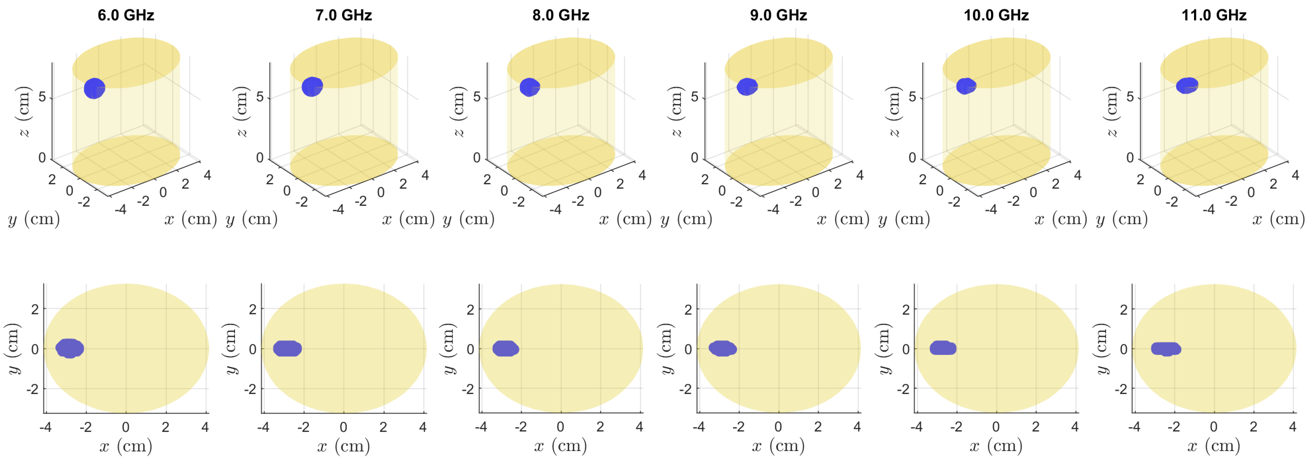

Figure 2. Single-frequency projections in the $6-11$ GHz range considering the multi-position approach, with the contaminant located in $\mathrm{L}_1 = (-2.8, 0, 7)$ cm.

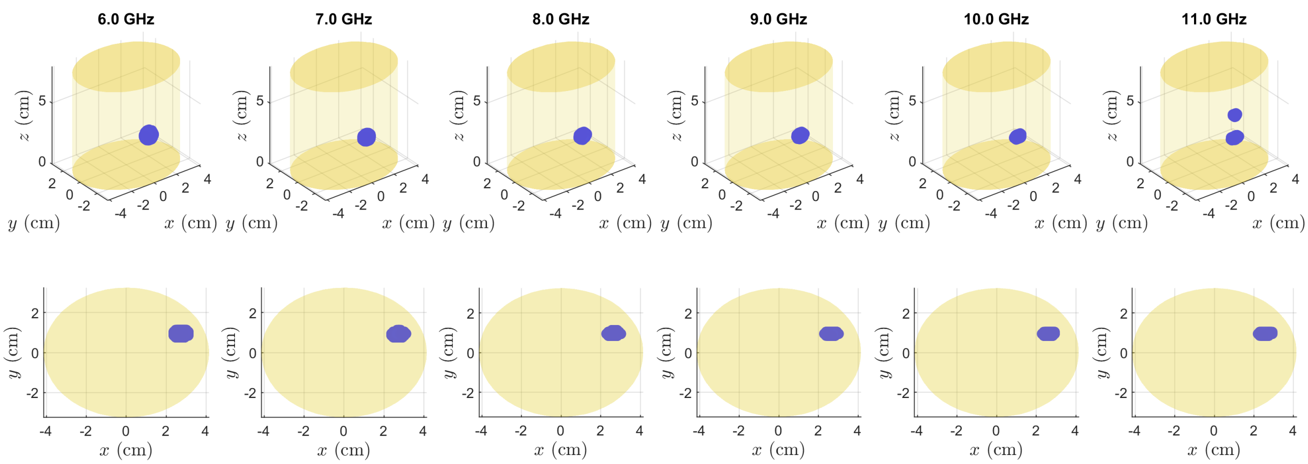

Figure 3. Single-frequency projections in the $6-11$ GHz range considering the multi-position approach, with the contaminant located in $\mathrm{L}_2 = (3, 1, 0.8)$ cm.

Equation (3) allows to reconstruct the 3D dielectric contrast map, through the differential scattering matrix, obtainable from simulations or measurements on real cases.

An important step, to be able to get then accurate reconstructions, is the assessment of the performance of the operator on synthetic data. This can be done directly obtaining case by case simulations on the contaminated scenarios, but the operation could be time-consuming. Therefore, in this paper, we use a strategy which allows to rapidly verify the quality of the images. Focusing on the right singular vectors $[v_n]$, these form an orthonormal basis for the row space of $[L]$. Hence, one can validate the capability of the basis set by projecting on it the expected dielectric contrast, $[\check{\chi}]$, as follows:

$$[\chi] = \sum_{n=1}^{T} \langle [\check{\chi}], [v_n] \rangle [v_n]. \tag{4}$$

The result is the synthetic reconstruction $[\chi]$, that corresponds to the *best* possible reconstruction in the considered functions' space $[v_n]$. Once the operator is retrieved from the simulation, the proposed process consists of just assigning the contrast values $[\check{\chi}]$ on the mesh grid and, then, performing the projections on the basis $[v_n]$ to compute $[\chi]$. This procedure does not require any further full-wave simulation, because the scattering matrices related to the contaminated scenario are not involved. Moreover, this method prevents including any numerical errors in the scattering matrix, deriving from the meshing process of the intrusion in the contaminated scenario, which depends on its position.

In cases when fictitious replicas arise during the reconstruction procedure of $[\chi]$, due to the limited capabilities of the basis $[v_n]$, we apply the frequency-based correction method, recently proposed in [9], to filter out the artifacts. We compute the $[\chi^{\mathrm{P}}]$ multi-frequency contrast as:

$$[\chi^{\mathrm{P}}] = \frac{\prod_{f=1}^{F} [\chi]_f}{\max \prod_{f=1}^{F} [\chi]_f}, \tag{5}$$

where the single-frequency reconstruction are marked with the label f, and F is the total number of available frequency points.

IV. Numerical results

We consider the scenario proposed in Fig. 1 to validate the system performance with a millimeter size spherical contaminant, placed within the investigation domain and illustrated with a black sphere in all the following figures. In particular, we explore locations which are poorly illuminated by the array, and result challenging for detection. Therefore, contaminants are placed in the corners of the container along the y-axis, to evaluate the $[L]$ operators performance under these conditions. The presented results consist of 3D maps of the dielectric contrast, expressed in magnitude and normalized with respect to its maximum value, rescaling it in a 0 to 1 range. The reconstructed binarized regions marked in blue represent the normalized dielectric contrast thresholded at 0.85 (corresponding to the values within the $15\,\%$ of the maximum).

Figure 2 shows the single-frequency *best* achievable reconstructions in the dynamic scenario for a contaminant placed in the top-left part of the jar. It is possible to observe that the reconstruction patterns are all able to correctly identify the contaminant position (the black dot representing the contaminant is always covered by the reconstructed dielectric contrast in blue), enlarging a bit its size. In Fig. 3, we explore the bottom-right corner of the jar, which is another challenging location. In this case, good results are also achieved, but for what concerns the image at 11 GHz, a ghost replica is reconstructed by the algorithm.

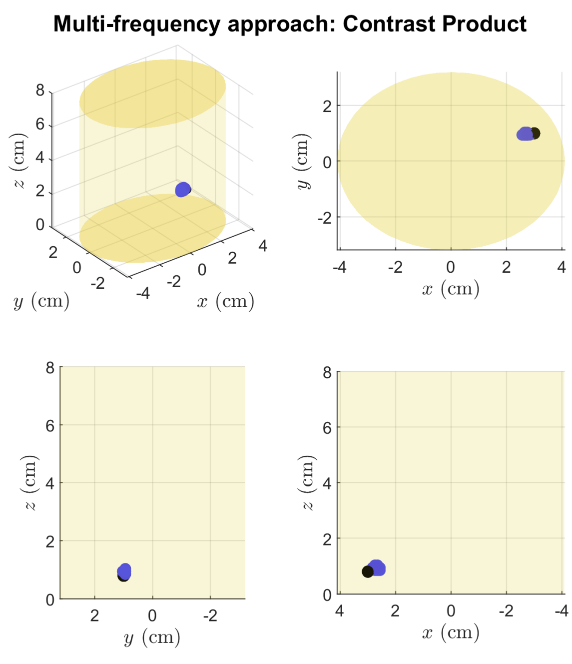

Figure 4. Multi-frequency projections with the contrast product method, obtained over the $6-11$ GHz range, considering the multi-position configuration, with the contaminant located in $\mathrm{L}_2=(3,1,0.8)$ cm.

To improve the reconstructed dielectric contrast, in Fig. 4, we illustrate the effect of a contrast product multi-frequency approach in filtering out the unwanted replica. It is applied by merging the results presented in Fig. 3. We can observe that the shape and location of the contaminant are improved, due to the focusing capabilities obtained by intersecting the single-frequency projections.

V. Conclusion and Perspectives

This work presents the numerical validation of a MWI food inspection system for oil-based products. The architecture setup, optimized with the EGRHS antennas, provides a good coverage of the tested item, while the projection feasibility check together with the multi-frequency approach ensure fast and accurate numerical dielectric contrast reconstructions.

Considering the promising results, future work will focus on the practical implementation of the system, evaluating its performance on real production lines. Additionally, including a realistic container model will enhance the system robustness.

Acknowledgment

This work is part of the project PNRR-NGEU which has received funding from the MUR – DM 117/2023. This research was supported in part by the project “INSIGHT-FOOD – An innovative microwave sensing system for the evaluation and monitoring of food quality and safety”, funded by the Italian Ministry of Foreign Affairs and International Cooperation (MAECI).

References

[1] M. Jelali and K. Papadopoulos, “Inline inspection of packaged food using microwave/terahertz sensing—an overview with focus on confectionery products,” *MDPI Processes*, vol. 12, pp. 1–21, 2024.

[2] J. A. Tobon Vasquez, R. Scapaticci, G. Turvani, M. Ricci, L. Farina, A. Litman, M. R. Casu, L. Crocco, and F. Vipiana, “Noninvasive inline food inspection via microwave imaging technology: An application example in the food industry,” *IEEE Antennas and Propagation Magazine*, vol. 62, no. 5, pp. 18–32, 2020.

[3] M. Ricci, J. A. T. Vasquez, R. Scapaticci, L. Crocco, and F. Vipiana, “Multi-antenna system for in-line food imaging at microwave frequencies,” *IEEE Transactions on Antennas and Propagation*, vol. 70, no. 8, pp. 7094–7105, 2022.

[4] N. Zeni, G. Bellizzi, L. Crocco, and M. Cavagnaro, “A compact antipodal vivaldi antenna for food investigation,” in *17th European Conference on Antennas and Propagation (EuCAP)*, 2023.

[5] N. K. Nikolova, *Introduction to Microwave Imaging*. Cambridge University Press, 2017.

[6] M. Bertero, P. Boccacci, and C. De Mol, *Introduction to inverse problems in imaging*. CRC press, 2021.

[7] J. F. González-Pardo, C. I. Maraloiu, J. A. Tobón Vasquez, M. Ricci, and F. Vipiana, “UWB horn antenna for food inspection via microwave imaging,” in *URSI EMTS 2025 25th International Symposium on Electromagnetic Theory*, 2025.

[8] S. Rashid, L. Jofre, A. Garrido, G. Gonzalez, Y. Ding, A. Aguasca, J. O’Callaghan, and J. Romeu, “3-D printed UWB microwave bodyscope for biomedical measurements,” *IEEE Antennas and Wireless Propagation Letters*, vol. 18, no. 4, p. 626–630, 2019.

[9] C. I. Maraloiu, J. A. T. Vasquez, M. Ricci, L. Crocco, and F. Vipiana, “Multi-frequency microwave imaging inspection for industrial food quality assessment,” in *2025 19th European Conference on Antennas and Propagation (EuCAP)*, 2025, pp. 1–4.